

Singular Perturbation Theory for DC-DC Converters and Application to PFC Converters

Jonathan W. Kimball, *Senior Member*

Philip T. Krein, *Fellow*

Grainger Center for Electric Machinery and Electromechanics
University of Illinois at Urbana-Champaign
1406 W. Green St., Urbana, IL 61801 USA

Abstract— Many control schemes for dc-dc converters begin with the assertion that inductor currents are “fast” states and capacitor voltages are “slow” states. This assertion must be true for power factor correction (PFC) converters to allow independent control of current and voltage. In the present work, singular perturbation theory is applied to boost converters to provide rigorous justification of the time scale separation. Krylov-Bogoliubov-Mitropolsky (KBM) averaging is used to include switching ripple effects. A relationship between inductance, capacitance, load resistance, and loss resistances derives from an analysis of an approximate model. Similar results hold for buck and buck-boost converters. An experimental boost converter and a simulated PFC boost support the derived requirement.

Keywords—singular perturbation, integral manifold, averaging, power factor correction.

I. INTRODUCTION

Frequently, controllers for dc-dc converters use two loops: an inner (“fast”) current loop and an outer (“slow”) voltage loop. The current loop can take many forms. In an analog controller, the most common approach is peak current mode, where the inductor current is compared to a reference to generate pulsewidth modulation (PWM) gate commands. Average current mode, hysteresis current control, and delta modulation are all well-known current control schemes. In the digital realm, several methods have been proposed [1-10], most of which fundamentally assume that capacitor voltage remains fixed for the duration of a switching cycle.

The current reference in a two-loop controller is determined through feedback on output voltage. If there is a separation in time scales between the current dynamics and voltage dynamics, the two loops can be designed independently. For example, power factor correction (PFC) converters use an outer loop to regulate voltage and an inner loop for current waveform tracking. The voltage loop determines the magnitude of the current waveform.

Singular perturbation theory [11] is a tool for formally partitioning a dynamic system into slow and fast variables. The two time scales differ by a factor of ϵ , which is small. The fast variables, denoted here as z , are related to the slow

This work was supported in part by the National Science Foundation under NSF Award ECS 06-21643.

variables, denoted as x , by an integral manifold (an algebraic relation) plus a small dynamic error η that is $O(\epsilon)$.

The present work starts with a switch-based piecewise-linear model of a boost converter, which is then normalized to show the variable relationships and identify suitable time-scale separation. Krylov-Bogoliubov-Mitropolsky (KBM) averaging allows the switched circuit configurations to yield a nonlinear time-invariant model that includes a ripple correction term. This model fits the standard form for singular perturbation analysis. An approximate model is shown to be suitable only if the converter parameters meet an additional constraint. An experimental converter demonstrates the effect of the additional constraint on dynamics. Finally, similar results are presented for buck and buck-boost converters.

II. SWITCHED LINEAR AND AVERAGED MODEL

A typical PFC boost converter is shown in Fig. 1. In the following analysis, v_{in} is treated generically as a disturbance input that could be dc, rectified ac, or any other shape. In terms of the physical variables, the converter dynamics are

$$\begin{aligned} \frac{dv_C}{dt} &= -\frac{1}{C(R+R_C)}v_C + h_2 \frac{R}{C(R+R_C)}i_L \\ \frac{di_L}{dt} &= -h_2 \frac{R}{L(R+R_C)}v_C - \frac{R_L + h_2(R\parallel R_C)}{L}i_L + \frac{v_{in}}{L} \end{aligned} \quad (1)$$

Here, h_2 represents the switching function of the diode. The model shown in (1) is for continuous conduction mode. Before proceeding, the variables are normalized. The designed output voltage is V_o , which corresponds to a nominal output

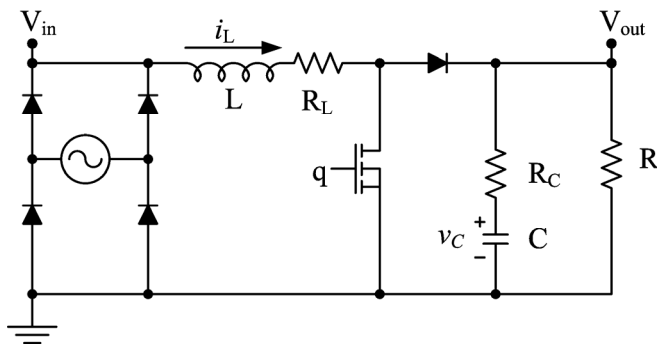


Fig. 1. Boost PFC Converter.

current $I_0 = V_0/R$. Let other values be

$$\begin{aligned}
\hat{v}_C &= \frac{v_C}{V_0} \\
\hat{i}_L &= \frac{i_L}{I_0} = \frac{i_L R}{V_0} \\
w &= \frac{v_{in}}{V_0} \\
u &= 1-d = \langle h_2 \rangle \\
\hat{i} &= \frac{t}{C(R+R_C)} \\
p &= \frac{T}{C(R+R_C)} \\
\delta_0 &= \frac{R_L}{R} \frac{R+R_C}{R} \\
\varepsilon &= \frac{L}{R^2 C}
\end{aligned} \tag{2}$$

The normalized state variables are \hat{v}_C and \hat{i}_L . The control input is really the duty ratio d , but the analysis is clearer using u . The disturbance input is now represented as w . Time is normalized to the capacitor time constant. The switching period T is converted to the new time scale to become p . The last two variables, δ_0 and ε , simplify the equations and will be important for the singular perturbation analysis in section III.

The normalized dynamic system is

$$\frac{d}{d\hat{t}} \begin{bmatrix} \hat{v}_C \\ \hat{i}_L \end{bmatrix} = \begin{bmatrix} -1 & h_2 \\ -h_2 & -\delta_0 + h_2 \frac{R_C}{R} \end{bmatrix} \begin{bmatrix} \hat{v}_C \\ \hat{i}_L \end{bmatrix} + \begin{bmatrix} 0 \\ \frac{R_C + R}{\varepsilon R} \end{bmatrix} w \tag{3}$$

This is still a switched system that is piecewise-linear in time. Singular perturbation analysis is based on a (possibly nonlinear) time invariant system. Typically, a ‘‘fast switching’’ assumption is invoked and state-space averaging is applied [12, 13]. More rigorously, KBM averaging can be applied [14-16]. In the KBM technique, a time-varying system

$$\dot{\xi} = \alpha \mathbf{F}(t, \xi) \tag{4}$$

is mapped to a time-invariant system

$$\dot{\mathbf{y}} = \alpha \mathbf{G}_1(\mathbf{y}) + \alpha^2 \mathbf{G}_2(\mathbf{y}) + \alpha^3 \mathbf{G}_3(\mathbf{y}) + \dots \tag{5}$$

The state vectors ξ and \mathbf{y} are related by a time-varying

transformation involving a power series of ripple functions

$$\xi(t) = \mathbf{y}(t) + \alpha \Psi_1(t, \mathbf{y}) + \alpha^2 \Psi_2(t, \mathbf{y}) + \dots \tag{6}$$

The algorithm given in [14-16] equates terms in powers of α to solve for \mathbf{G}_i and Ψ_i . The Mathematica script in [16] has been updated and expanded, and is reported in Appendix A. For a basic dc-dc converter, \mathbf{G}_1 is the conventional state-space average. For this boost converter, \mathbf{G}_2 is zero. \mathbf{G}_3 gives a non-zero correction term proportional to $(p/\varepsilon)^2$. The nonlinear time-invariant system in \mathbf{y} is given in (7) for terms through \mathbf{G}_3 . Higher terms diminish rapidly provided p/ε is small.

The remainder of the analysis could proceed from (7). If the converter is operating in continuous conduction mode, the

leading coefficient $\frac{1}{12} \left(\frac{u(1-u)p}{\varepsilon} \right)^2$ is less than or equal to

one, and all the terms it multiplies are small. As a result, the terms that come from \mathbf{G}_3 are generally small and have little impact on dynamics, although they do change the steady-state operating point slightly. \mathbf{G}_3 will be left out for now to make the symbolic analysis easier to follow, but the complete expression will be addressed in Section IV.

III. SINGULAR PERTURBATION MODEL

A singularly perturbed system can be separated into a fast subsystem and a slow subsystem. The standard form of the dynamic system is [11]

$$\begin{aligned}
\dot{\mathbf{x}} &= \mathbf{f}(\mathbf{x}, \mathbf{z}, \mathbf{u}, \mathbf{w}, \varepsilon) \\
\varepsilon \dot{\mathbf{z}} &= \mathbf{g}(\mathbf{x}, \mathbf{z}, \mathbf{u}, \mathbf{w}, \varepsilon)
\end{aligned} \tag{8}$$

An exogenous input \mathbf{u} and a disturbance input \mathbf{w} are included. All variables must be normalized and all coefficients in \mathbf{f} and \mathbf{g} must be $O(1)$. If $\varepsilon \ll 1$, then the two subsystems can be analyzed separately. The fast variables are \mathbf{z} , and the principle is that their behavior can be analyzed with \mathbf{x} assumed to be quasi-static. The slow variables are \mathbf{x} , which can be analyzed with \mathbf{z} set to an algebraic relation (an integral manifold).

In the boost converter system (7), the slow variable is $x=y_1$ and the fast variable is $z=y_2$. Leaving out \mathbf{G}_3 and higher-order contributions, the system can be written as

$$\begin{aligned}
\frac{dx}{d\hat{t}} &= uz - x \\
\varepsilon \frac{dz}{d\hat{t}} &= \frac{R+R_C}{R} w - ux - \left(\delta_0 + \frac{R_C}{R} u \right) z
\end{aligned} \tag{9}$$

All variables are normalized as in (2). All of the coefficients

$$\begin{aligned}
\frac{dy_1}{d\hat{t}} &= uy_2 - y_1 - \frac{1}{12} \left(\frac{u(1-u)p}{\varepsilon} \right)^2 \left(y_1 (\delta_0 - \varepsilon) + \frac{R_C}{R} \frac{R+R_C}{R} w \right) \\
\varepsilon \frac{dy_2}{d\hat{t}} &= \frac{R+R_C}{R} w - uy_1 - \left(\delta_0 + \frac{R_C}{R} u \right) y_2 + \frac{1}{12} \left(\frac{u(1-u)p}{\varepsilon} \right)^2 \left(y_1 \frac{R_C}{R} (\delta_0 - \varepsilon) + y_2 \varepsilon (\delta_0 - \varepsilon) + \frac{R+R_C}{R} w \left(\frac{R_C^2}{R^2} - \varepsilon \right) \right)
\end{aligned} \tag{7}$$

on the right hand sides are $O(1)$ except the coefficient of z in g (the right-hand side of the second equation in (9)). Define this coefficient to be

$$\delta(u) = \delta_0 + \frac{R_C}{R}u \quad (10)$$

All of the terms that make up $\delta(u)$ are related to losses, which should be small in a practical converter. Therefore, further analysis is needed.

The next step is to construct an approximate model,

$$z = \varphi_0 + \varepsilon\varphi_1 + \eta \quad (11)$$

The φ terms are algebraic and represent the integral manifold; φ_0 is the solution when $\varepsilon = 0$ and φ_1 is a first-order correction. The η term represents the off-manifold dynamics. For this system, η is governed by

$$\varepsilon \frac{d\eta}{dt} = -\delta(u)\eta + \frac{\varepsilon\eta u^2}{\delta(u)} \quad (12)$$

This approximate model is only valid if the η dynamics are stable, that is, if η decays to zero from an arbitrary initial condition. Since u is bounded ($u \in [0,1]$) and exogenous, the stability requirement can be written as

$$\varepsilon u^2 < \delta^2(u) \quad (13)$$

Typically, a converter must operate over a wide range of u as input voltage changes. A more general, necessary requirement for stability is

$$\varepsilon < \delta_0^2 \quad (14)$$

If the converter design satisfies (14), then there are indeed two time scales. If time scale separation is important for the application, (14) can be treated as a design objective or as an optimization constraint.

Simply put, (14) requires nonzero losses to ensure time scale separation. A useful analogy is a linear system. Without adequate damping, a second-order system will have complex conjugate eigenvalues. With sufficient damping, the eigenvalues will be real and distinct. Similarly, for a boost converter with adequate losses, the inductor current characteristic time scale (like an eigenvalue) will be much faster and distinct from the capacitor voltage time scale.

In most converters, $R_C \ll R$, so $\delta_0 = R_L/R$. Substituting this approximation in (14) and simplifying, the requirement becomes

$$\sqrt{\frac{L}{C}} < R_L \quad (15)$$

for time scale separation. This is a convenient form for quickly determining whether the converter design is appropriate for two-loop control. The load resistance does not

TABLE 1. BASIC CONVERTER PARAMETERS.

L	657 μ H	C	77 μ F
R_L	584 m Ω	R_C	381 m Ω
MOSFET	IRF3710	Diode	MBR1545CT
ε	8.5×10^{-4}	δ_0	5.9×10^{-3}
Frequency	25 kHz	ρ	5.2×10^{-3}
R	100 Ω		

appear in (15). The two time scales change as load resistance changes, but the existence of separation between them does not. The requirement in (15) is the same as requiring the quality factor Q of the RLC circuit composed of the inductor, its resistance, and the idealized capacitor to be less than 1.

IV. EXPERIMENTAL VERIFICATION

A simple boost converter was constructed to demonstrate the time scale phenomena. The main parameters are summarized in Table 1. A low-power 12 V to 36 V application was chosen for simplicity of experimental setup. MOSFET resistance is lumped into R_L . The converter was operated open-loop through a duty cycle step from 67% to 64%. With the parameters in Table 1, (14) is not satisfied. Fig. 2 shows output voltage and inductor current dynamics through the duty cycle step. Note the underdamped transient and coupling between current and voltage behavior.

Next, resistance (2 Ω) was added in series with the inductor. Now, ε is unchanged, $\delta_0 = 0.026$, and (14) is satisfied. Fig. 3 shows the response to the same duty ratio step as Fig. 2. The response is essentially that of a pair of decoupled first-order systems. Most of the current dynamics visible on this time scale come from the integral manifold $\varphi_0 + \varepsilon\varphi_1$. The extra loss is not desired, of course, and degrades efficiency.

Another approach for satisfying (14) is to add output

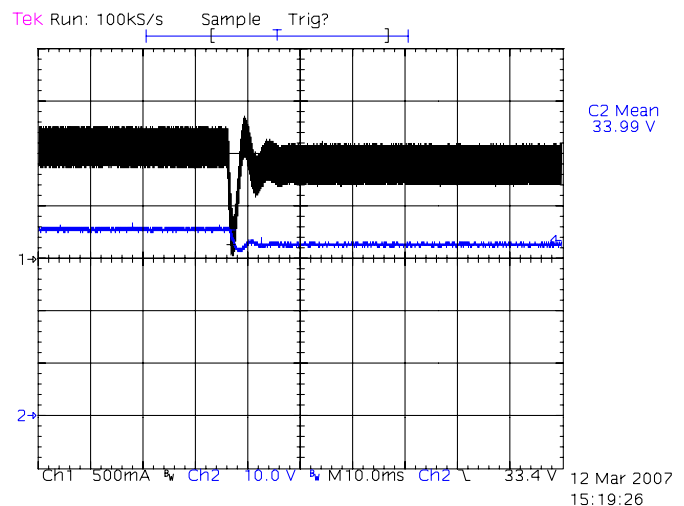


Fig. 2. Experimental duty cycle step (67% to 64%) with original converter. Note second-order behavior. Channel 1, inductor current, 500 mA/div; channel 2, output voltage, 10 V/div; horizontal, 10 ms/div.

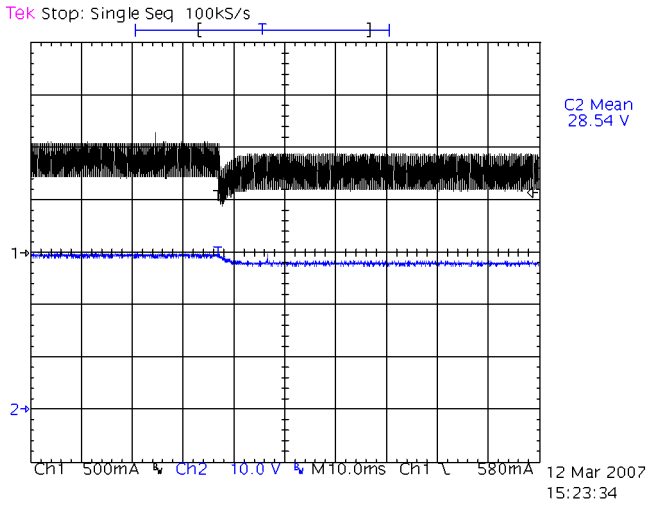


Fig. 3. Experimental duty cycle step (67% to 64%) with added resistance in inductor ($2\ \Omega$). Note decoupled behavior. Channel 1, inductor current, 500 mA/div; channel 2, output voltage, 10 V/div; horizontal, 10 ms/div.

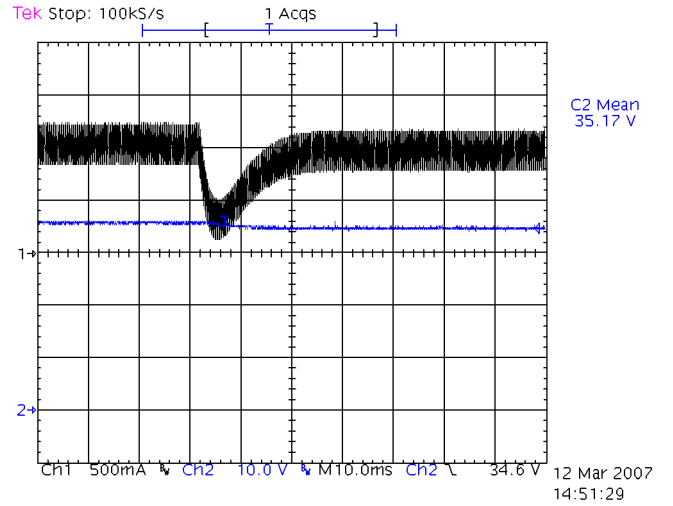


Fig. 4. Experimental duty cycle step (67% to 66%) with added output capacitance ($2200\ \mu\text{F}$). Note decoupled behavior. Channel 1, inductor current, 500 mA/div; channel 2, output voltage, 10 V/div; horizontal, 10 ms/div.

capacitance. In this converter, a much larger capacitance of $2200\ \mu\text{F}$ will decrease ε to 3.16×10^{-5} . The response to a smaller duty cycle step (67% to 66%) is shown in Fig. 4. Now the “fast” dynamics are more obvious, but decoupling is still evident. During the first 5 ms after the step, the current drops quickly. For the rest of the transient, the current follows the integral manifold as the voltage decays to its steady-state value. High efficiency is retained while time-scale separation is achieved.

While higher-order terms in the KBM average greatly complicate symbolic analysis, numerical analysis can easily include \mathbf{G}_3 , and higher order terms are typically very small. The converter is operating in continuous conduction mode. As indicated above, the leading coefficient for \mathbf{G}_3 is less than 1:

$$\frac{1}{12} \left(\frac{u(1-u)p}{\varepsilon} \right)^2 = 0.151 \quad (16)$$

The complete system of (7) is now

$$\begin{aligned} \frac{dy_1}{dt} &= 0.33y_2 - 1.00087y_1 - 5.7 \times 10^{-4}w \\ \varepsilon \frac{dy_2}{dt} &= 1.0038w - 0.33y_1 - 0.00712y_2 \end{aligned} \quad (17)$$

for the large-capacitance case, with other parameters from Table 1. The φ terms in the approximate model do not have a significant impact. The η dynamic equation can be found numerically and can include \mathbf{G}_3 terms, to give

$$\begin{aligned} \varepsilon \frac{d\eta}{dt} \Big|_{base} &= 6.9856\eta - 1.30 \times 10^{-13}y_1 - 5.19 \times 10^{-13}w \\ \varepsilon \frac{d\eta}{dt} \Big|_{add C} &= -209.6\eta - 1.21 \times 10^{-12}y_1 - 3.95 \times 10^{-12}w \end{aligned} \quad (18)$$

The first dynamic equation, corresponding to the base converter design, does not have a stable equilibrium. The second dynamic equation includes additional capacitance and has a stable equilibrium near zero. The presence of y_1 and w terms means that the off-manifold dynamics decay to a small non-zero value. The overall behavior still exhibits two-time-scale characteristics.

V. BUCK AND BUCK-BOOST CONVERTERS

A buck converter is much simpler than a boost converter for this analysis procedure. In the KBM analysis, all terms above \mathbf{G}_1 vanish. The averaged model in standard form for singular perturbation analysis is

$$\begin{aligned} \frac{dx}{dt} &= z - x \\ \varepsilon \frac{dz}{dt} &= \frac{R + R_c}{R} (1-u)w - x - \left(\delta_0 + \frac{R_c}{R} \right) z \end{aligned} \quad (19)$$

For clarity, the same variable definitions were used as in the boost case. Again, the approximate model can be found, where the off-manifold dynamics are

$$\begin{aligned} \varepsilon \frac{d\eta}{dt} &= \frac{\varepsilon\eta}{\delta} - \delta\eta \\ \delta &= \delta_0 + \frac{R_c}{R} \end{aligned} \quad (20)$$

As in the boost converter, the approximate model is only valid if the η dynamics are stable, or

$$\varepsilon < \delta^2 \quad (21)$$

The input u no longer matters. Otherwise, the time scale separation criteria are exactly the same as the boost converter.

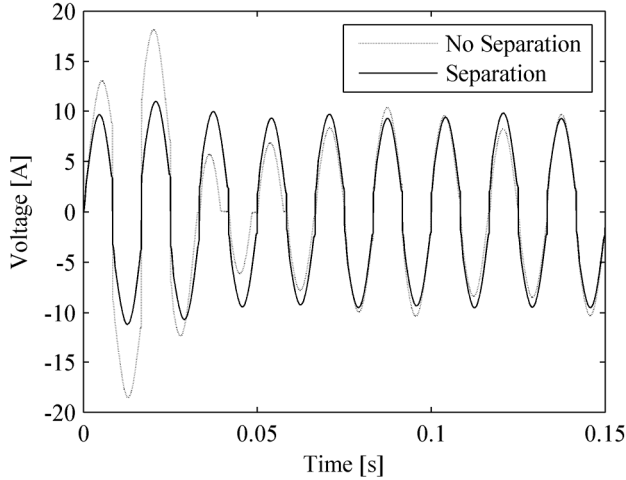


Fig. 5. Simulated PFC boost converter. Line current shown for two cases. For both, $L = 5$ mH, $C = 5$ mF, $T = 13.33$ μ s, $R = 50$ Ω . R_L varies from 80 m Ω (no separation) to 1.28 Ω (separation).

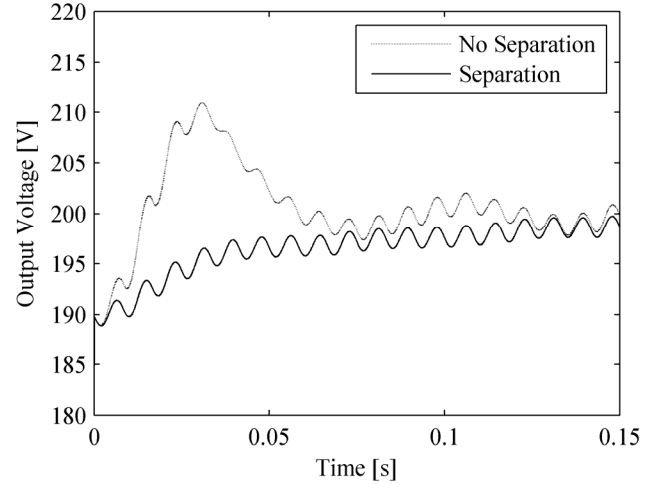


Fig. 6. Simulated PFC boost converter. Output (capacitor) voltage shown for two cases. See Fig. 5 for more details.

The buck-boost converter is more complicated. As in the boost converter, the higher-order terms (particularly \mathbf{G}_3) in the KBM average are non-zero and are similarly proportional to $(p/\varepsilon)^2$. Neglecting the contribution of \mathbf{G}_3 , the state-space-averaged model in standard form for singular perturbation analysis is

$$\begin{aligned} \frac{dx}{dt} &= uz - x \\ \varepsilon \frac{dz}{dt} &= \frac{R+R_C}{R}(1-u)w - ux - \left(\delta_0 + \frac{R_C}{R}u \right) z \end{aligned} \quad (22)$$

The off-manifold dynamics in the approximate model are identical to a boost converter (12) and all of the same conditions in (13) through (15) apply.

VI. APPLICATION TO PFC BOOST CONVERTERS

PFC boost converters rely on time scale separation for stable operation. A simulation has been constructed to demonstrate the effect of R_L on dynamic performance. The control law combines feedback and feedforward,

$$u = \frac{V_{in}}{V_0 + 10 \int (V_0 - v_C) dt} \quad (23)$$

Despite the lack of explicit current control, this control produces current that is nearly sinusoidal. Figs. 5 and 6 show the line current and bus voltage start-up transients, respectively, for two converters with different R_L . With R_L too small, there is no separation, and a second-order oscillation with overshoot is observed. With additional damping, the current magnitude and average voltage show first-order behavior. The estimated efficiency with separation exceeds 93%. A larger output capacitor would enable separation with less damping and higher efficiency.

VII. SUMMARY AND CONCLUSIONS

Time scale separation is often assumed for inductor current and capacitor voltage dynamics in dc-dc converters. A singular perturbation analysis shows that this assertion is true if the converter construction satisfies a key condition. Essentially, the losses in the converter must be high enough to damp the inductor dynamics. Models of and requirements for buck, boost, and buck-boost converters are similar.

In particular, time scale separation is critical for power factor correction (PFC) applications. Otherwise, voltage dynamics affect current harmonics and the control problem becomes much more complicated. Fortunately, a typical PFC application requires a large capacitor to absorb the double-frequency power ripple. Large capacitance results in small ε , so most practical converters will satisfy the necessary conditions.

REFERENCES

- [1] P. Athalye, D. Maksimović, and R. Erickson, "Variable-frequency predictive digital current mode control," *IEEE Power Electronics Letters*, vol. 2, pp. 113-116, Dec. 2004.
- [2] S. Bibian and H. Jin, "High performance predictive dead-beat digital controller for DC power supplies," *IEEE Transactions on Power Electronics*, vol. 17, pp. 420-427, May 2002.
- [3] F. Blaabjerg, P. C. Kjaer, P. O. Rasmussen, and C. Cossar, "Improved digital current control methods in switched reluctance motor drives," *IEEE Transactions on Power Electronics*, vol. 14, pp. 563-572, May 1999.
- [4] S. Chattopadhyay, V. Ramanarayanan, and V. Jayashankar, "A predictive switching modulator for current mode control of high power factor boost rectifier," *IEEE Transactions on Power Electronics*, vol. 18, pp. 114-123, Jan. 2003.
- [5] J. Chen, A. Prodić, R. Erickson, and D. Maksimović, "Predictive digital current programmed control," *IEEE Transactions on Power Electronics*, vol. 18, pp. 411-419, Jan. 2003.
- [6] D. G. Holmes and D. A. Martin, "Implementation of a direct digital predictive current controller for single and three phase voltage source inverters," in *Proc. IEEE Industry Applications Conference*, 1996, pp. 906-913.

- [7] Y.-S. Jung, "Small-signal model-based design of digital current-mode control," *IEE Proceedings-Electric Power Applications*, vol. 152, pp. 871-877, July 2005.
- [8] P. Mattavelli, "Digital control of dc-dc boost converters with inductor current estimation," in *Proc. Applied Power Electronics Conference*, 2004, pp. 74-80.
- [9] C.-T. Pan, Y.-S. Huang, and C.-Y. Li, "An error bounded current controller with constant sampling frequency," *IEEE Transactions on Power Electronics*, vol. 19, pp. 739-747, May 2004.
- [10] H. Peng and D. Maksimović, "Digital current-mode controller for dc-dc converters," in *Proc. Applied Power Electronics Conference*, 2005, pp. 899-905.
- [11] P. V. Kokotović, H. K. Khalil, and J. O'Reilly, *Singular Perturbation Methods in Control: Analysis and Design*. London: Academic, 1986.
- [12] R. D. Middlebrook and S. Čuk, "A general unified approach to modeling switching converter power stages," in *Proc. IEEE Power Electronics Specialists Conference*, 1976, pp. 18-34.
- [13] R. D. Middlebrook and S. Čuk, "A general unified approach to modeling switching dc-to-dc converters in discontinuous conduction mode," in *Proc. IEEE Power Electronics Specialists Conference*, 1977, pp. 36-57.
- [14] P. T. Krein, J. Bentsman, R. M. Bass, and B. L. Lesieutre, "On the use of averaging for the analysis of power electronic systems," *IEEE Transactions on Power Electronics*, vol. 5, pp. 182-190, April 1990.
- [15] B. Lehman and R. M. Bass, "Switching frequency dependent averaged models for PWM dc-dc converters," *IEEE Transactions on Power Electronics*, vol. 11, pp. 89-98, Jan. 1996.
- [16] P. T. Krein and R. M. Bass, "A new approach to fast simulation of periodically switching power converters," in *Proc. Industry Applications Society Annual Meeting*, 1990, pp. 1185-1189.

```
KBAlgorithm[rhs,zerovec,zeromat,zerovec,zeromat]
G1=Simplify[G]
 $\Psi$ 1=Simplify[psi];
 $\Psi$ avg1 = Simplify[psiavg];
 $\Psi$ di1 = Simplify[psidi];
```

```
apsi=Table[a[[j]]. $\Psi$ 1[[j]],{j,nconfi}];
KBAlgorithm[apsi,G1,zeromat,zerovec, $\Psi$ 1]
G2=Simplify[G]
 $\Psi$ 2=Simplify[psi];
```

```
apsi=Table[a[[j]]. $\Psi$ 2[[j]],{j,nconfi}];
KBAlgorithm[apsi,g2, $\Psi$ 2,g1, $\Psi$ 1]
G3=Simplify[G]
```

```
f = G1[[1]]+G3[[1]]
g =  $\epsilon$ *(G1[[2]]+G3[[2]])
```

```
intermediate = Solve[g==0,iLnorm]
 $\varphi$ 0 = (iLnorm /. intermediate)[[1]]
 $\varphi$ 1 = (1/D[g,iLnorm])*(D[ $\varphi$ 0,vCnorm])*(f /. iLnorm  $\rightarrow$   $\varphi$ 0)
 $\eta$ rhs = (g /. iLnorm  $\rightarrow$  ( $\varphi$ 0 +  $\epsilon$ * $\varphi$ 1 +  $\eta$ ))- $\epsilon$ *(D[ $\varphi$ 0,vCnorm])*(f /. iLnorm  $\rightarrow$  ( $\varphi$ 0+ $\eta$ ));
infinitef = Simplify[simple $\eta$ rhs /. p  $\rightarrow$  0]
```

APPENDIX A: MATHEMATICA SCRIPT

```
x={vCnorm,iLnorm};
T={0,duty*p,p};
nconfi=2;
amat={{-1,h2},{-h2/ $\epsilon$ ,-( $\delta$ 0+h2*Rc/R)/ $\epsilon$ }};
bmat={0,(Rc+R)*w/( $\epsilon$ *R)};
n=Length[x];
a={(amat/.{h1 $\rightarrow$ 1,h2 $\rightarrow$ 0}),(amat/.{h1 $\rightarrow$ 0,h2 $\rightarrow$ 1})};
b={(bmat/.{h1 $\rightarrow$ 1,h2 $\rightarrow$ 0}),(bmat/.{h1 $\rightarrow$ 0,h2 $\rightarrow$ 1})};

rhs=Table[a[[i]].x+b[[i]],{i,nconfi}];

AVERAGE[f_]:=Cancel[(1/p)
Sum[Integrate[f[[id0]],{t,T[[id0]],T[[id0+1]]}],{id0,nconfi}]];

PDER[fv_v_]:=Table[D[fv[[id1]],v[[jd1]]],{id1,n},{jd1,n}];

KBAlgorithm[rhspsi_Gold_psiold_Golder_psiolder_]:=Block[{i}
,
G=AVERAGE[rhspsi];
psidi=Simplify[Table[Integrate[rhspsi[[i]]-G-
PDER[psiolder[[i]],x].Gold-
PDER[psiold[[i]],x].Golder,t],{i,nconfi}]];
psibc={psidi[[1]]};
Do[AppendTo[psibc,Cancel[psidi[[i]]+(psibc[[i-1]]/.t $\rightarrow$ T[[i]])-
(psidi[[i]]/.t $\rightarrow$ T[[i]])],{i,2,nconfi}];
psiavg=AVERAGE[psibc];
psi=Table[psibc[[i]]-psiavg,{i,nconfi}];];

zerovec=Table[0,{i,n}];
zeromat=Table[zerovec,{i,nconfi}];
```